RAL-TR-2000-043

RESONANT MAGNETIC X-RAY DIFFRACTION

Sean Langridge and Stephen W. Lovesey

Rutherford Appleton Laboratory, Chilton, Didcot, Oxfordshire OX11 0QX, United Kingdom

Email: s.w.lovesey@rl.ac.uk
s.langridge@rl.ac.uk

Keywords: Magnetism, x-ray, magnetic structures, magnetic phase transitions, lanthanide, actinide, surface and interfacial magnetism.

Contents:

1. Introduction

Traditionally, the technique of choice for the study at an atomic level of detail of magnetic structures, correlations and excitations has been magnetic neutron scattering (Lovesey 1987). Reviews of the neutron probe in the study of magnetism have been presented by Rossat-Mignod (1987) and Stirling and McEwen (1987). Two features of the neutron are pivotal in attaining this status; (a) the wavelength of a thermal neutron is a good match to the spacing of ions in a crystal and (b) the neutron carries a magnetic moment and it interacts strongly with electronic magnetic moments. However, the ready availability of sophisticated diffraction instruments supplied with an intense beam of photons, from a synchrotron source, beckons a reappraisal of the status quo.

1.1 Historical overview

The interaction between a photon and the spin of an electron was elegantly described by Gell-Mann and Goldberger in 1954; thus far, the interaction with the orbital moment of an ion has defied a similar description (Durbin 1998). Platzman and Tzoar (1970) appear to be the first advocates of x-ray scattering as a tool to investigate magnetic properties of materials, and the first experimental observation of the magnetic Bragg diffraction of x-rays was published by DeBergevin and Brunel two years later. A landmark paper in the exploitation of x-ray magnetic Bragg diffraction was by DeBergevin and Brunel and it appeared in print almost a decade after their pioneer experimental study. In the landmark paper one finds a thorough treatment of the diffraction of x-rays by electronic spin and orbital magnetic moments, and the relationship between x-ray and neutron magnetic diffraction. Although we will not be discussing the inelastic and magnetic scattering of x-rays it is fitting in a brief history to mention that the first experimental observation of magnetic

Compton scattering was reported in 1976 by Sakai and Ôno; recent reviews of the subject are given by Sakai (1996) and Lovesey and Collins (1996). Returning to theoretical work on magnetic x-ray scattering, the scattering length correct to second-order in the relatively small relativistic effects responsible for this scattering is completely understood (Bhatt et al. 1983, Grotch et al. 1983). To-date, the result for the scattering length correct at the first level of approximation appears to adequately describe experimental data.

Whilst the magnetic diffraction of x-rays was most certainly seen as scientifically interesting, the weak nature of the magnetic scattering is a handicap that limited the applicability of the non-resonant technique to a wider range of systems. The situation changed with the combination of the availability of intense and tuneable beams of x-rays, from synchrotron sources, and the discovery of the resonant enhancement of the x-ray magnetic diffraction in ferromagnetic Ni by Namikawa *et al.* (1985) and in antiferromagnetic Ho by Gibbs and co-workers (1988).

The large increase in the magnetic signal (of order 50 in the lanthanides and 10^6 in the actinides) as the incident x-ray energy is tuned through the relevant absorption edge provides a new tool for the study of magnetism. X-ray Resonant Magnetic Scattering (XRMS) not only complements neutron scattering measurements but extends the study of magnetism, particularly in the realm of thin film, interfacial magnetism and multicomponent systems, as discussed in sections 2 and 3, into new and exciting areas of research. The enhancement of x-ray diffraction arises from the promotion of a core electron to an empty excited state above the Fermi energy, which then decays with a characteristic lifetime through the emission of an elastically scattered photon. The largest enhancements observed to date are at the M edges of the

actinides. Since the magnetic signal is specific to the elemental absorption edge the probe provides an *element specific* technique. Tuning the incident photon energy then maps out the spin polarisation of the empty density of states. In dipole events (E1), for transition and lanthanide metals the L edges couple the spin-orbit split *p* states to the *d* states and in the actinides the M edges couple the core *d* states directly to the magnetic 5*f* bands. A schematic of the L-edge resonance is shown in figure 1.

Experimentally, the XRMS technique has several attractive features:

- The probe is element and band selective.
- The inherent small emittance and high brightness of modern synchrotron sources gives excellent wave-vector resolution and intense scattering, essential in the study of magnetic phase transitions.
- x-ray beam sizes of order several hundred microns at the sample position allow the study of small single-crystal samples.
- The high degree of controllability of the incident polarisation (both linear and circular) gives ready access to the polarisation dependent terms in the resonant x-ray cross-section, which can be successfully applied to differentiate between magnetic and charge scattering.

In the following sections, we have addressed the theoretical framework for XRMS and highlighted certain areas of intense research interest. For a more complete treatise on magnetic x-ray scattering and absorption the reader is referred to Lovesey and Collins (1996) and Gibbs *et al.* (1999)

1.2 Orientation

By way of orientation to experimental studies reviewed in subsequent sections of the chapter, we start with a brief discussion of the interactions responsible for

scattering neutrons and x-rays from magnetic materials and then comment on resonant diffraction.

In the case of neutrons, the fundamental strength of the interaction for scattering from electronic magnetic moments is the classical electron radius $r_e = \alpha$. The effective strength depends on the magnitude of the electronic moment, and for a lanthanide ion with total angular moment J and a Landé factor g it can be taken to be $r_e\, g\, J$. One notes that the strength of scattering of neutrons from a magnetic moment is similar to the strength of scattering from a nucleus.

Turning to x-rays (Lovesey and Collins, 1996 and Gibbs *et al*., 1999), the magnetic scattering is weak compared to Thomson scattering which has a cross-section = r_e^2. To say more than this we shall separately consider the scattering of hard x-rays and scattering enhanced by an atomic resonance. For Bragg diffraction of very hard x-rays from planes of reflection separated by a distance d the effective strength is $r_e(\lambda_o/d)\ (g - 1)J$ where the Compton wavelength $\lambda_o = (2\pi r_e/\alpha) =$ 0.00243nm. This effective strength is small compared to r_e, and it depends on the spin moment of the ion and not the orbital moment. The last observation brings us face to face with a useful difference between the interaction with a magnetic moment of a neutron and a photon which was first identified by DeBergevin and Brunel (1981). The interaction of a neutron with a moment is described by $g\ \mathbf{J} = (\mathbf{L} + 2\mathbf{S})$, provided it is not deflected through a very large angle.

As we have already seen, hard x-rays are diffracted by the spin moment = $(g - 1)\ \mathbf{J}$. With other scattering conditions x-ray diffraction provides direct information on the orbital moment of a magnetic ion. One such case is resonant x-ray diffraction at the K edge which has been discussed by Lovesey and Knight (2000). The strength of

resonant diffraction depends on several properties of the resonant ion including, of course, the width in energy of the resonance level. By and large, the quality of the information obtained using resonant x-ray diffraction is not as good as the information obtained using hard x-rays and beams of neutrons, because here interactions are very simple and in cross-sections they contribute constant factors. The motivation to use resonant x-ray scattering, and to develop a theoretical framework for the interpretation of data, comes from the significant size of signals and the possibility of extracting information not obtainable using other experimental techniques. Future prospects include more frequent use of inelastic resonant x-ray scattering (Lovesey and Balcar, 1996 and Hill *et al*., 1998).

Cross-sections for Bragg diffraction are usually expressed in terms of unit-cell structure factors, which are dimensionless quantities. The spin density structure factor describes both the configuration and orientation of the spin moments in a magnetic unit-cell, and it is denoted here by $\mathbf{F}_s(\mathbf{k})$. In Bragg diffraction, the scattering wave-vector, $\mathbf{k}$, matches a reciprocal lattice vector with magnitude $(2\pi/d)$. Let the magnetic ions be at positions in the unit cell defined by $\mathbf{d}_j$, and denote the atomic spin form factor by $f_j(\mathbf{k})$. Using this notation,

$$\mathbf{F}_s(\mathbf{k}) = \sum_j \left\langle \mathbf{S}_j \right\rangle f_j(\mathbf{k}) \exp(i\mathbf{k}\cdot\mathbf{d}_j) \qquad (1)$$

where $\langle \mathbf{S} \rangle$ is the mean value, equivalent to the time average, of the spin. In the diffraction of hard x-rays one observes the component of $\mathbf{F}_s(\mathbf{k})$ which is perpendicular to the plane of scattering, depicted in Fig. 2, and this component is denoted by $F_s^z(\mathbf{k})$ (Brunel and DeBergevin, 1981). For very hard x-rays, with a wavelength << *d*, the cross-section per unit cell is,

$$r_e^2 \left| F_c(\mathbf{k}) + i(\lambda_o / d) F_s^z(\mathbf{k}) \right|^2 . \qquad (2)$$

Here, $F_c(\mathbf{k})$ is the charge unit-cell structure factor and the normalization makes $F_c(0)$ the total charge (in units of $|e|$) in a unit cell. If F_c and F_s^z are both purely real, and different from zero, the magnetic contribution in (2) is weighted relative to the charge contribution by the very small quantity $(\lambda_o/d)^2$. It is quite possible for F_c to be a complex quantity in which case there is a term in the cross-section of order (λ_o/d) and proportional to F_s^z (Im.F_c). The 90° phase shift in (2) between the charge and magnetic amplitudes indicates that circular polarisation in the primary beam can induce an interference of the two amplitudes, akin to what happens when F_c is not purely real (Lovesey and Collins 1996).

The observation about using circular polarisation to pick out the magnetic signal prompts us to say a few words about magnetic Compton scattering (Sakai, 1996). Although an incoherent and inelastic scattering process, Compton scattering and hard x-ray Bragg diffraction have common features. For one thing, the Compton profile arises from the spin density of unpaired electrons, and there is no information to be had on orbital magnetism (Lovesey and Collins, 1996). Secondly, circular polarisation in the primary beam is routinely used to separate the charge and magnetic contributions to the profile.

The structure factor for magnetic neutron Bragg diffraction, $\mathbf{F}(\mathbf{k})$, is quite similar to (1). In place of the spin moment in (1) one has the projection of the magnetic moment $\mu = \langle \mathbf{L} + 2\mathbf{S} \rangle$ perpendicular to $\mathbf{k}$, namely, $\{\mathbf{k} \times (\boldsymbol{\mu} \times \mathbf{k})\}/k^2$, and the spin form factor is replaced by the magnetic moment form factor. (Here and in (1) we omit the Debye-Waller factor, which is also a decreasing function of k.) If the moment configuration is collinear and $\mathbf{k}$ is parallel to the preferred magnetic axis the

cross-section is zero. This selection rule is found to be extremely useful in determining the components of a magnetic ordering wave-vector.

We close this section by further discussing resonant processes. The discussion is made in terms of the resonant contribution to the scattering length, denoted by *f*. Absorption, and attendant dichroism and birefringence, are described by the imaginary part of $\langle f \rangle$ evaluated for the geometry of forward scattering. The cross-section for resonant Bragg diffraction is proportional to $|\langle f \rangle|^2$. Hence, absorption and scattering are two sides of one coin (Lovesey and Collins, 1996).

Let us label intermediate, and excited states engaged in the resonance event by η. These are non-equilibrium states of the resonant ion which have a life-time = $(\hbar/\gamma_\eta)$, and they are of no interest to us apart from their contribution to *f*. A schematic view of the resonant event is shown in Fig. 1. If the energy of the primary x-rays and the resonance energy are *E* and Δ_η, respectively, a contribution to $\langle f \rangle$ evaluated at the first level of approximation has the form,

$$\sum_\mu p_\mu \sum_\eta \frac{\langle \mu | B^+ | \eta \rangle \langle \eta | B | \mu \rangle}{\left(E - \Delta_\eta + \frac{\mathrm{i}}{2} \gamma_\eta \right)} \qquad (3)$$

where p_μ is the thermal (Boltzmann) factor for the equilibrium state of the target sample labelled μ. To date, the experimental evidence is that the transition operator *B* is electric. Certainly, the ratio of magnetic to electric absorption events is of the order of the fine-structure constant which leads us to expect a small, and possibly negligible, magnetic contribution to the scattering length.

For electric dipole (E1) events $B = R^{\alpha}$ and for electric quadrupole (E2) events $B = R^{\alpha}R^{\beta}$ where **R** is the position operator and α and β label Cartesian components. As functions of the Cartesian labels, E1 events contain 9 quantities and E2 events contain 81 quantities. Since $\langle f \rangle$ is a bulk quantity Neumann's Principle applies to it, and the symmetry elements for $\langle f \rangle$ include the symmetry elements of the point group of the crystal. In consequence, the number of independent quantities is usually reduced. For example, an E2 event involving an ion occupying a site with symmetry 2/m (monoclinic, C_{2h}) in a paramagnetic material is described by 13 independent quantities, and for hexagonal systems there are just 5 independent quantities (Nye 1960, Birss 1964). Even smaller numbers of independent quantities are required to specify structure factors for charge-forbidden reflections (Templeton and Templeton 1994, Nagano *et al*. 1996).

There are a variety of methods for calculating the independent quantities and relating them to physical properties of the resonant ion. The methods can be put in one of two classes, namely numerical and analytical. For the moment, at least, numerical methods are of limited value, e.g. atomic (Garcia *et al*. 2000) band structure (Ebert 1996) calculations are performed at zero temperature. As might be expected, to make progress with analytical methods some approximations are required. One method decouples the numerator and energy denominators in (3), and employs an atomic model for the matrix elements of *B*. Beyond this there is no further approximation (Carra and Thole 1994, Lovesey and Balcar 1997). In the case of dichroism, which is related to Im. $\langle f \rangle$, one obtains exact results for the integrated spectrum, and the results are usually called sum rules (see van der Laan 1994, and references therein). It should be emphasised that, after decoupling the numerator and

energy denominator one does not sum over all intermediate states and invoke the closure relation $\sum|\eta\rangle\langle\eta| = 1,$ because this is altogether a step too far and no magnetic (time odd) quantities survive. In place of (3) one works with the expression,

$$\frac{G(\mathbf{k})}{(E - \Delta + \frac{\mathrm{i}}{2}\Gamma)} \tag{4}$$

where it is understood that E and Δ almost match. Evidently, $G(\mathbf{k})$ is the integrated weight attached to the resonance in question, and one finds,

$$G(\mathbf{k}) = \sum_{\mathrm{j}} \left\langle Z(\mathrm{j}) \right\rangle \exp\left(\mathrm{i}\mathbf{k}\cdot\mathbf{d}_{\mathrm{j}}\right), \tag{5}$$

the atomic quantities in $\langle Z(\mathrm{j})\rangle$ relate to the valence shell which accepts the photo-excited core electron.

Because one is using an atomic model, results for $\langle Z\rangle$ are expressed in terms of spherical tensors, examples of which include spherical harmonics. By working with Cartesian components, mentioned earlier on, one is led to manipulate Cartesian tensors and matrices (Nye 1960, Birss 1964, Nagano *et al*. 1996). It can be shown that the matrix approach is equivalent to working with sums of spherical tensors in which the coefficients are determined by symmetry properties of the corresponding matrices, e.g. invariance with respect to certain rotations and time reversal.

Again using an E2 event as an example, and considering K-edge absorption ($1s \rightarrow 3d$), $\langle Z(\mathrm{j})\rangle$ is the sum of five scalar products,

$$\left\langle Z(\mathrm{j}) \right\rangle = \sum_{K=0}^{4} (2K+1)^{1/2}\, \mathbf{H}^{(K)} . \left\langle \mathbf{T}^{(K)}(\mathrm{j}) \right\rangle \tag{6}$$

in which K is the rank of a tensor, the spherical tensor $\mathbf{H}^{(K)}$ is determined by the conditions of the incident and diffracted beams, and $\langle \mathbf{T}^{(K)}\rangle$ is proportional to an orbital

moment of the 3*d* valence shell, e.g. $\langle \mathbf{T}^{(1)} \rangle = \langle \mathbf{L} \rangle / \sqrt{30}$ and $\langle \mathbf{T}^{(4)} \rangle = \langle \Upsilon \rangle / 18\sqrt{70}$ where $\langle \mathbf{L} \rangle$ is the orbital moment and $\langle \Upsilon \rangle$ is the corresponding hexadecapole. (For an electric dipole (E1) event $K = 0$, 1 and 2.) It is to be noted that $\langle \mathbf{T}^{(K)} \rangle$ is axial-like, i.e. it is invariant with respect to inversion of the coordinates, and changing the direction of time multiplies $\langle \mathbf{T}^{(K)} \rangle$ by $(-1)^K$ and reverses the polarity of the magnetic field (applied or spontaneous magnetic order). Selection rules on the photon polarisation are derived from $\mathbf{H}^{(K)}$, and they are not pursued here (Lovesey and Knight, 2000).

Charge-forbidden reflections arise either from spatial anisotropy (and this scattering is often called Templeton and Templeton scattering after its discoverers) or the spontaneous ordering of magnetic moments with a configuration different from that of a simple ferromagnet. Stemming from their very nature, the interpretation of charge-forbidden reflections can reveal details of magnetic properties of a material. We will cite some features of charge forbidden reflections in diffraction by resonant ions which occupy sites that have low spatial symmetry, e.g. V_2O_3, hematite, iron pyrite and ferrous niobate ($FeNb_2O_6$).

Just like a spherical harmonic, each spherical tensor of rank K has $(2K + 1)$ components and we label a component by an integer m, $-K \leq m \leq K$, which is denoted by $\left\langle T_m^{(K)} \right\rangle$. Due to a coupling of structural and orbital properties in a diffraction signal (h, k, l) there can be selection rules on K, m and the Miller indices. In the case of V_2O_3 (Lovesey and Knight, 2000) charge-forbidden reflections satisfy K odd and $h + m$ even and spatial symmetry restricts m to the values 0, ± 3, to a good approximation. From these selection rules it follows that charge-forbidden reflections with h odd have $m = \pm 3$ and for an E2 absorption event diffraction is due to $\left\langle T_{\pm 3}^{(3)} \right\rangle$, which contains the orbital octupole moment. In particular, a reflection with h odd is

not at all sensitive to E1 enhanced diffraction because for an E1 event the maximum value of K is 2.

Spatial anisotropy in the valence shell of the resonant ion is manifest in azimuthal-angle scans, in which the crystal is rotated about the Bragg wave-vector (Brunel and DeBergevin 1981, Nagano *et al*. 1996). If the principal axes coincide with the crystallographic axes an azimuthal-angle scan can mesh with a rotation-axis symmetry. An example of this behaviour is found in scans performed on hematite (Finklestein *et al*. 1992); a three-fold axis of rotation passes through the site occupied by the ferric ion and the azimuthal-angle scan displays a six-fold periodicity as a direct consequence of this symmetry. A similar effect is not expected when the orbital moment is subjugate to the spin moment in the Néel state and the preferred magnetic axis is canted away from the crystallographic axes. The same reasoning applies for a paramagnetic material in which the principal axis is not a crystal axis. An example of the quite complicated azimuthal-angle scan observed with such a material is found in diffraction by iron pyrite (FeS_2). The resonant iron ions occupy a site with symmetry $\bar{3}(C_{3i})$ and the principal axis is [111]. Azimuthal-angle scans with a Bragg wave-vector (011) for FeS_2 (Kokubun *et al*. 1998) do not display a clear signature of the three-fold axis of rotation, e.g. scans are not six-fold periodic as in the case of hematite.

Experimental data collected on magnetically ordered vanadium sesquioxide (Paolasini *et al*. 1999) have been interpreted (Lovesey and Knight 2000) in terms of a model in which the spin and orbital moments are independent degrees of freedom. The orbital magnetism is referred to the trigonal structure which describes the high-temperature crystal structure, whereas the observed magnetic moment in the ordered phase is inclined at 71° to the trigonal axis. Bragg wave-vectors for charge-forbidden

reflections are not parallel to the trigonal axis and, understandably, azimuthal-angle scans possess no immediately obvious signature of the three-fold axis of rotation.

Lastly, we note that circular polarisation can be created in diffraction of a completely linearly polarized beam of X-rays if amplitudes for the rotated ($\pi'\sigma$) and unrotated ($\sigma'\sigma$) channels of scattering are shifted in phase such that the imaginary part of the product of the amplitudes is different from zero. One possible scenario which gives rise to this effect is pure magnetic scattering in ($\sigma'\sigma$) and purely charge scattering in ($\pi'\sigma$). For this case, amplitudes for the two channels are 90° out of phase. Yet another possibility arises with complicated configurations of the moments, leading to pure magnetic scattering in both ($\sigma'\sigma$) and ($\pi'\sigma$) and complex phase factors coming from the actual nature of the configuration. The conjugate process to the creation of circular polarisation, just discussed, is dependence of the Bragg intensity to circular polarisation in the incident beam of x-rays (Lovesey and Collins, 1996).

We now turn to review some recent experimental studies, highlighting both the capabilities of the XRMS technique and the resulting new science.

2. Magnetic Structures, Electron Polarisation and Phase Transitions

2.1 Rare-Earth magnetism

Of the magnetic elements, arguably the simplest to understand are the rare-earths. The electronic structure consists of un-filled 4*f* levels and a 5*d* state which contains either one or no electrons. These 4*f* levels lie deep within the 5*s* and 5*p* shells and are strongly screened by the large outer charge density. The 4*f* electrons are highly localised and a signature of this is the existence of well defined crystal field (CF) levels. For the localised rare-earths the spin-orbit coupling is greater than the CF

potential which means that the *LS* coupling scheme is still valid. The 4*f* orbitals are too localised for direct exchange between neighbouring 4*f* ions. In this limit, the coupling is between the 4*f* and conduction electron states. As a result the 4*f* electron interaction is indirect through the polarisation of the conduction electrons. This interaction, first developed by Ruderman and Kittel and later by Kasuya and Yoshida, the *RKKY* interaction, is not localised near the 4*f* ion but is long range and oscillatory. The indirect nature of the exchange means that the sign and magnitude of the exchange interaction can change from site to site resulting in sinusoidal and helical structures in the heavier rare-earths (greater than half-filled 4*f* shell) and even more complicated structures in the lighter rare-earths (less than half-filled 4*f* shell). For example, a helical structure is formed at the Néel temperature in Tb, Dy and Ho whilst below 106K Sm has a complicated *c*-axis modulation with ordered hexagonal sites but disordered cubic sites. A complete review of rare-earth magnetism has been presented by Jensen and Mackintosh (1991).

As previously stated, the first observation of XRMS in an antiferromagnetic system was in Ho. Elemental Ho has the hexagonal close packed (hcp) structure with a large magnetic moment of $10.6\mu_B$ per ion. In the ground state Ho has ten 4*f* electrons and three electrons in the conduction states. The energy widths are 2eV and 5-10eV, respectively, for the 4*f* and conduction states. Below the magnetic ordering temperature,138K, magnetic satellites parallel to the crystallographic *c*-axis are observed which is consistent with a simple helical modulation. Within the basal plane the moments are aligned ferromagnetically and rotate from plane to plane along the *c*-axis. This turn angle is proportional to the magnetic modulation wave-vector, τ. Neutron scattering measurements suggested that τ varied smoothly with temperature below the ordering temperature with an incommensurate modulation (from $\tau \sim 0.3c^*$ to

$\tau \sim 1/6c^*$ at 20K). Below 20K, Ho develops a conical magnetic structure with a ferromagnetic component along the *c*-axis. The intrinsic high wave-vector resolution of x-ray scattering allowed Gibbs and co-workers (1985) to use non-resonant magnetic x-ray scattering measurements to observe that in certain temperature ranges the modulation wave-vector locks to commensurate wave-vectors. In addition to the magnetic satellites additional reflections were observed, which through their polarisation dependence, were found to have a charge character. Such satellites result from "spin slips" in which single layers rather than two coupled layers rotate to bring the system close to a commensurate modulation. Subsequently, both x-ray and neutron measurements have revealed such spin slip structures to be a common feature of rare-earth systems. The large Ho moment gives non-resonant magnetic x-ray intensity with typical count rates of $50sec^{-1}$. The high wave-vector resolution coupled with the ability to separate charge from magnetic scattering through the polarisation dependence has resulted in a far greater understanding of the magnetic ordering in the rare-earth series.

Subsequently, Gibbs and co-workers (1988) observed resonant magnetic scattering by tuning the incident photon energy to the Ho L_{III} edge (8067eV). At the maximum intensity of the resonance (8070eV) an enhancement in the magnetic scattering of factor ~50 relative to the non-resonant signal was observed. In addition, higher harmonic reflections were observed (τ,2τ,3τ and 4τ) at resonance. A closer examination of the energy dependence of the resonant lineshape also revealed the presence of two contributions to the resonance with differing polarisation dependencies. Hannon *et al.* (1988) developed an *atomic* model to describe these results. As discussed in section 1.2, the enhancements arose from *electric* multi-polar transitions and successfully described both the higher order harmonics and their

polarisation dependence. The maximum in the resonant enhancement above the absorption edge is consistent with electric dipolar transitions whilst for quadrupole the maximum enhancement is several eV below the edge, reflecting the stronger Coulomb coupling of the core 2*p* and 4*f* states. For the case of Ho, the τ and 2τ harmonics are allowed in dipolar transitions coupling the core 2*p* states to 5*d* conduction states. In quadrupole, 2*p* to 4*f* electric transitions result in τ, 2τ, 3τ and 4τ higher satellites. The integrated magnetic intensity for the harmonics is shown in figure 3 and is in good agreement with the atomic model presented by Hannon *et al.* A detailed report (Gibbs, D. *et al.* 1991) gives a very complete description of the Ho work.

The relative strength of the magnetic scattering means that x-rays can now be used to *solve* complicated and unknown magnetic structures which may be difficult or inaccessible to more conventional neutron techniques, because of, for example, strong neutron absorption or small single crystal volume *etc*. The most complete x-ray study of a rare-earth magnetic structure has been in Nd. It should be noted that Nd has been studied for over 30years *via* neutron techniques. Nd has a double hcp structure with two Nd sites with local hexagonal and cubic site symmetry. Below 19.9K the hexagonal sites order with a single sinusoidally modulated phase. Cooling further increases the number of ordering wave-vectors from one to four in the lowest temperature phase. Forgan *et al* (1996) studied Nd in the temperature range 11.5-20K. In the range ~1K below T_N, Nd adopts a single ordering wave-vector (single-k) along {100} type directions. Below this there is a weakly first order transition to a double-k structure in which the moments move away from the symmetry directions. The existence of a double-k structure was only implied through neutron observations of weak harmonics, or the application of a symmetry breaking magnetic field. The advantage of the x-ray technique is the small sampling volume of order $0.01mm^3$

compared to several mm^3 in the neutron case. In a multi-domain sample 12 magnetic satellites would be expected. Only four satellites were observed consistent with a single antiferromagnetic domain. This represents a significant advantage since the presence of multi-domains can prevent a unique structure determination. Interestingly, no sign of lock in transitions was observed. Watson *et al.* (1998) extended these measurements and produced a full analysis of the Nd magnetic structure at 10K by analysing 96 magnetic reflections.

The additional information obtainable by combining resonant and non-resonant magnetic diffraction measurements has been demonstrated by Detlefs *et al.* (1996) in a series of rare-earth (RNi_2B_2C, R=rare-earth) compounds. These measurements benefit from the increased wave-vector resolution and the ability to look at systems which for neutron measurements require isotopic substitution because of the high neutron absorption cross-section *e.g.* Gd and Sm.

In addition to the XRMS properties highlighted in section 1.1, there is significant benefits in combining XRMS measurements with neutron diffraction measurements. The complementarity of the two techniques brings significant insight, as demonstrated in the case of Ho and more recently in complex multi-component systems. To illustrate this complementarity consider the case of the ternary intermettalic; $DyFe_4Al_8$. The resonant enhancement of the x-ray technique allows the possibility of selectively accessing the magnetism in this multi-component system, whilst the neutron technique allows *absolute* moment determination with high precision. Of interest is the interaction of the shielded *4f* electrons through the rare-earth *5d* states and the *3d* magnetism of the transition metal. Initial studies employing, neutron powder diffraction, susceptibility and Mössbauer spectroscopy suggested time-dependent and irreversible behaviour characteristic of a spin glass. For the

magnetic structure, antiferromagnetic order was believed to exist below ~180K with a further transition below 40K. To separate the *3d* and rare-earth contributions to the magnetization, XRMS measurements were performed at the Dy L_{III} edge. Temperature dependent resonant magnetic scattering was observed at a modulation wave-vector of $(\tau,\tau,0)$ with τ~0.133 reciprocal lattice units, as shown in figure 4.

Concentrating on the x-ray data collected at the Dy L_{III} resonance the onset of magnetic ordering appears at ~170K which then increases slowly until a dramatic increase below 50K. This measurement, in a dipole event, is probing the Dy *5d* states ($2p_{3/2} \rightarrow 5d_{5/2}$). This, then, is clear direct evidence for an induced polarisation of the *5d* states. Below 20K the increase in intensity is the enhanced *5d* polarisation driven by the development of an ordered Dy *4f* moment. This ability to select specific electronic states is one of the most powerful attributes of the XRMS probe. Fortunately, the neutron probe although not band selective is able to distinguish between the Dy and Fe contributions. Using the Bragg diffraction selection rules for the $ThMn_{12}$ structure, reflections which have either a magnetic contribution from Dy (e.g. (121)+τ) or a combination of Dy and Fe (e.g. (110)+τ) can be separated. This data is overlaid on figure 4. It is now apparent that it is the polarisation of the Fe that initially drives the *5d* polarisation of the Dy. The neutron interaction, being sensitive to the magnitude of the total magnetic moment, is clearly not sufficiently sensitive to measure the small induced *5d* polarisation and therefore no neutron intensity is observed above ~40K for Dy-only type reflections.

By analysing the polarisation and **k** dependence of the resonant magnetic x-ray scattering at the Dy L_{III} resonance for two configurations of the sample geometry (Langridge *et al.* 1999), confirmation of a simple cycloidal arrangement of the Dy moments was established and a high precision determination of the magnetic ordering

wave-vectors. To fully analyse the magnetic structure requires the use of zero-field spherical neutron polarimetry (Brown *et al*. 1993). By controlling the incident and scattered neutron polarisation the detailed magnetic structure was obtained and it is shown in figure 5 for T=17K. An analysis of the full neutron polarisation confirmed and refined the structure indicated by the XRMS measurements. With a detailed understanding of the resonant x-ray scattering length, studies of this type will be more prevalent (Detlefs *et al*. 1997, Watson *et al*. 1998). The ability to separate the contributions from multi-component systems has recently been eloquently demonstrated in the high T_c superconductor series. The non-superconducting member of the R-123 family, $PrBa_2Cu_3O_{6.92}$ has attracted considerable attention because of the role of stripe ordering in the suppression of the superconductivity. XRMS measurements at the Pr L_{II} edge show incommensurate magnetic ordering. XRMS measurements at the Cu K-edge display quadrupole magnetic scattering, indicating the presence of a Cu moment, which is commensurate below the Néel temperature but which are driven to a double-k ordering with an incommensurate and commensurate component by the ordering of the Pr moments (Hill *et al.* 2000). These measurements would appear to discount the stripe ordering suppression.

Whilst the above studies have concentrated on using the XRMS technique for the study of phase transitions, magnetic structure solutions *etc.* there exists the exciting possibility that the resonant process will act as a spectroscopy for the magnetic states. To characterise the enhancements a branching ratio can be defined. For the rare-earth resonances the ratio is created with the integrated intensities at the L_{III} to the L_{II}. As was reported by Hill *et al.* (1995) there appears to be a trend in the branching ratio as the 4*f* shell is filled. For the light rare-earths the maximum enhancement occurs at the L_{II} edge, whilst for the heavy rare-earths the maximum

occurs at the L_{III}. A review of experimentally observed branching ratios is presented by Watson *et al.* (1996). Clearly, the number of 4*f* electrons is not the only factor as the light rare-earth Sm has a maximum in the enhancement at the L_{III} edge. Further deviations away from the atomic like description of the resonant process are highlighted in elemental Nd and the undoped parent super-conductor $NdCu_2O_4$ in which the branching ratio changes from 6 to ~100 respectively. Further observations of temperature-dependent branching ratios by Langridge *et al.* (1999) have led to an extension of the isolated ion approach, which would give rise to a temperature-independent branching ratio, to include solid state effects, namely the antiferromagnetic ordering and the metallic nature of the system under investigation. Whilst it is experimentally challenging, to reliably measure branching ratios given the large energy dependent change in sample absorption, and a theoretical challenge, to calculate the radial matrix elements in complicated systems, this has the possibility of a new spectroscopy for the magnetic states.

2.2Actinide Magnetism

The actinide series, characterised by a gradual filling of the 5*f* band, has attracted considerable experimental and theoretical interest as examples of strongly correlated electron systems. In the actinides the 5*f* level is close to the Fermi energy and the CF potential is close to the spin-orbit potential so there is an absence of well defined CF levels. This absence can be related to strong hybridisation between the 5*f* electrons and the *d* and *s* conduction electrons as well as the *p* and *d* states of the anion. This hybridisation leads to 5*f* bandwidths that are significantly lower than the localised 4*f* systems. The conclusion to be drawn from this is that the actinides lie somewhere between the localised 4*f* and the itinerant behaviour of the transition metal

elements. Significantly, the heavier actinides are not available in quantities suitable for neutron diffraction therefore opening the possibility of new studies using XRMS.

The first actinide to be studied using XRMS was UAs (Isaacs E.D. *et al.* 1989). In a dipole transition at the actinide M edges electrons are excited to the 5*f* state and large resonant enhancements are expected. UAs has a simple rocksalt structure which orders in a single-k antiferromagnetic type-I structure below 127K and subsequently a double-k, type-IA structure at 63K. Although experimentally challenging given the high x-ray absorption at <4keV and the long wavelength x-rays limiting the amount of reciprocal space accessible, three M edge resonances (M_{III}, M_{IV} and M_V) were observed and modelled as the sum of three dipole oscillators as suggested by Hannon *et al*. (1988). In the light actinides the M_{IV} resonance is the strongest given that this involves transitions to the $5f_{5/2}$ shell. Starting from the axiom that the energy width of the resonance is inversely proportional to the lifetime of the excited state it should, in principle, be possible to study the decay mechanism for the excited state, as well as any departures from Lorentzian type behaviour due to exchange broadening *etc*. Unfortunately, experimental energy resolution and crystal mosaic prevented any direct observation of such effects.

Whilst neutron scattering has made huge contributions to actinide research the difficulty in obtaining single crystal samples in sufficient volume has limited the study of the heavier actinides. The first measurements on trans-uranium systems were made by Langridge *et al.* (1994) on NpAs with a sample mass of <1mg as shown in figure 6. More recently the trans-uranium work has been extended to include Np-U solid solutions (Lidström *et al.* 2000) and NpO_2 which, unlike the magnetic structure of UO_2, has been unresolved for over 30years. Specific heat measurements on NpO_2 in 1953 revealed the existence of magnetic order below 25K as expected for a

Kramers ion with an odd number of 5*f* electrons. The confirmation of the magnetic structure was not forthcoming, possibly due to the small mass of single crystal available. Mannix *et al.* (1999) have reported XRMS measurements on the magnetic structure of NpO_2 with an estimated Np moment of $<0.1\mu_B$/atom. Using the polarisation and wave-vector dependence of the M_{IV} edge (λ=0.322nm) resonance an antiferromagnetic arrangement with the long range ordered Np moment parallel to the ordering wave-vector and adopting a triple-k structure was proposed. Unfortunately, it is not currently possible to reliably connect the observed XRMS intensity with absolute magnetic moments. Particularly in the case of the actinides, where the sample absorption is very high for photon energies <4keV (~$4.5\mu m^{-1}$ for the M_{IV} Np resonance), the x-ray penetration is low. This leads to two important considerations: the sampling volume is restricted to typically 100-200nm *i.e.* near-surface and the probe coherence has to be considered. The limited penetration depth provides a near-surface sensitivity which has to be considered if one allows the possibility of surface ordering different to that found in the bulk (as may be probed by the neutron technique or high energy photons for example). Indeed, Paixão *et al.* (1993) have reported near-surface ordering in $U_{0.85}Th_{0.15}Sb$ different to that observed in the bulk. The importance of the probe coherence and the absorption co-efficient is particularly evident in the actinide series in which the sample absorption is large. Indeed, when the incident photon coherence-length approaches the absorption length one can no longer ignore the finite photon coherence volume (Bernhoeft *et al.* 1998,1999) and only consider finite-size and resolution effects. This has important implications for the reliable measurement of actinide branching ratios and their comparison with advanced crystal-field calculations, and also in integrated intensity measurements as demonstrated in NpO_2.

The huge intensities and excellent wave-vector resolution of XRMS has also benefited the study of magnetic phase transitions and critical phenomena. A review of work both in the rare-earths and actinide has been presented by Stirling and Cooper (1999).

2.3 Transition Metal Magnetism

Transition metal magnetism has attracted much interest because of both a fundamental understanding of magnetism in itinerant systems and for the widespread technology based upon them. Unfortunately for XRMS, the largest resonant enhancements are expected for the L and M edges (*e.g.* Fe L_{III} 706.8eV) which in a dipole event couple to the magnetic 3*d* states. At such low energies it is not usually possible to satisfy the Bragg diffraction condition. This is not the case for multilayer structures, as discussed in section 3.1. Because of this the accessible resonance is the K edge which couples, in a dipole event 1*s* to 4*p* states. The localised core level is not spin-orbit split, the induced polarisation on the delocalised 4*p* band is likely to be small and so only small enhancements are expected. Nevertheless the high synchrotron brightness has led to several studies, particularly in the oxides. At the present time, studies of NiO (Hill *et al.* 1997) and CoO (Neubeck *et al.* 1999) have been reported. For NiO a factor of two enhancement was observed at the Ni K edge. The energy dependence of the scattering confirmed its origins in quadrupolar transitions 1*s* to 3*d*, with the large polarisation of the 3*d* band compensating for weak quadrupolar matrix elements. No enhancement was observed at the dipole-allowed transition. For CoO both dipolar and quadrupolar transitions have been observed. The observation of the quadrupolar scattering implies a large orbital moment (Lovesey,

1998), as in the case of NiO. It is interesting to compare this result with L=0 systems such as $RbMnF_3$ (Stunault *et al.* 1999).

We conclude this section by noting that, as described in section 1.2, the ground state of many strongly correlated systems are controlled not only by the magnetic degrees of freedom but may also include charge and orbital ordering. The resonant enhancement of the scattering allowed the first direct observation of both charge and orbital ordering (Murakami *et al.* 1998) in the layered perovskite, $La_{0.5}Sr_{1.5}MnO_4$. The exciting prospect is that such measurements will lead to a far greater understanding of the interplay between magnetism, charge and orbital ordering as reported by Zimmermann *et al.* (1999).

3. Surface and Interfacial Magnetism

3.1 Multilayers

Determining the properties and morphology of buried layers and interfaces remains an important experimental problem in solid-state science. Many of the technological end-products of this science are based on thin-film devices, which consist of a series of such layers. Characterisation of the physical microstructure and degree of the disorder of these films is commonly carried out by reflectivity, diffraction and diffuse scattering studies. Theoretical models for analysing such data are well advanced.

The past few years has seen intense activity in the development of magnetic devices for data storage, ultra-low field sensing and quantum computing applications. In such systems, a thorough knowledge of the magnetic microstructure is required. There are two main scattering techniques that can be used to this end: neutron diffraction and resonant magnetic x-ray diffraction. Before addressing the study of

surface magnetism, and the role of magnetic disorder, we consider XRMS in the study of multilayer systems. XRMS has been used to study the magnetic structure in thin magnetic layers and more recently the induced polarisation in magnetic/non-magnetic systems. Importantly the photon-in, photon-out nature of the experiment means that the applied magnetic field does not affect the measurements. So far, the studies have concentrated on transition metal and rare-earth multilayers, but we anticipate that this will extend to actinide systems in the near future.

Conveniently, x-ray wavelengths associated with the transition metal resonances match the layer thickness typically found in multilayer systems, so resonant Bragg diffraction measurements are possible. In addition, by coupling the diffraction measurements with magnetic circular dichroism allows a *quantitative* measure of the magnetic moments through application of the sum rules mentioned in section 1.2.

Recently, Ishimatsu *et al.* (1999) (and references therein) have reported in detail on the Fe/Gd system. Fe/Gd is a complex system exhibiting aligned and twisted states, depending on the strength of the applied field, as measured by ^{57}Fe Mössbauer and neutron scattering. Unfortunately, the Mössbauer technique is only sensitive to the Fe, and neutron technique cannot separate the Fe and Gd contributions. It had been suggested that the Gd magnetisation is non-uniform over a lengthscale of ~5nm. Using XRMS scattering, with circularly polarised photons at the Gd L-edge, a strong interfacial polarisation of the Gd was observed decaying to a minimum in the middle of the layer as shown in figure 7. The element-specific nature of the probe has also been employed to study the propagation of magnetic coupling in rare-earth superlattices across non-magnetic spacer layers. This coupling is believed to arise from a spin-density wave in the conduction band of the non-magnetic spacer.

Goff *et al.* (1999,2000) have demonstrated the existence of the spin-density wave in the non-magnetic spacer, Pr of a Nd/Pr multilayer. The constituent rare-earth resonances are shown in figure 8. An analysis of the observed wave-vector dependent intensity then allows a determination of the induced polarisation within the Pr layers.

3.2 Surface Magnetism

In recent years, there has been significant interest in assessing the magnetic order at surfaces and in thin-film magnetism. Given the break in crystal symmetry at the surface one might expect to observe magnetic structures and critical behaviour different to those found in the bulk. The experimental difficulty is that the surface charge scattering is typically 5 orders of magnitude weaker than the bulk scattering. For this reason, high brightness synchrotron grazing incidence x-ray scattering techniques are well advanced, allowing a well defined characterisation of the surface. The magnetic intensity is reduced relative to charge diffraction by 5-6 orders of magnitude and so one requires the XRMS enhancement to observe any magnetic contribution from the surface.

The influence of the surface on diffraction studies is to produce truncation rods, which are parallel to the surface normal. Measurements of the intensity variation along these rods then allow a determination of the charge structure near the surface (Feidenhans'l, 1989) on the atomic level of detail. For specular rods there is no in-plane component of the momentum transfer, and the information contained relates to the change in charge density perpendicular to the surface. For rods with an in-plane momentum transfer, information on the in-plane structure can be extracted as discussed in section 3.3. By analogy, truncation rods containing a magnetic contribution allow the magnetic surface to be characterised. Questions such as the atomic layer variation in the *element specific* magnetisation profile near to the surface,

the surface magnetic ordering and interfacial magnetic roughness can now be addressed.

To study the surface magnetisation profile, Ferrer *et al.* (1996) made XRMS measurements at the ferromagnetic surface of Co_3Pt. "Conventional" grazing incidence x-ray diffraction was performed on the Co_3Pt (111) surface revealing a disordered surface unit cell with the Pt concentration rising to 0.60 at the top layer. By tuning the incident x-ray energy to the L_{III} Pt absorption edge (11.564keV) the scattering length contains a significant magnetic contribution arising from electric dipolar transitions from core states to the narrow exchange-split Pt *5d* band. Reversing the sample magnetisation relative to the incident linear photon polarisation gives an asymmetry ratio which has a maximum at the resonance energy. Following the asymmetry ratio along the truncation rod allows the magnetic surface structure to be studied. The conclusion of the study was that, the surface Pt polarisation is approximately a factor two smaller than that in the bulk of the sample, and obvious explanation being the reduced number of nearest neighbour Co atoms in the surface.

The huge enhancement of the XRMS signal in actinide systems ($>10^6$), coupled with the large resonant absorption, makes such systems amenable to surface studies. As an example, we consider UO_2. Bulk UO_2 (Fraser, 1965) exhibits a discontinuous transition to a triple-**k** magnetic structure below T_N=30.2K. This is illustrated by the solid circles for the magnetic (001) Bragg reflection in figure 8. For glancing incidence geometry at the U M_{IV} resonance (3.728keV) the surface sensitivity is of order 3nm and, conversely, the temperature dependence of the (01L) magnetic truncation rod shows a continuous transition (Watson *et al.* 1996). Such differences have been observed in *structural* order-disorder transitions (see for example Reichert *et al.* 1995). However, a quantitative description of the magnetic

order-disorder transition remains unresolved. Potentially, these measurements can be expanded to include the role of magnetically "dead" layers at the surface and to identify the multi-**k** surface ordering which is not accessible through any other technique. The penetrating power of the neutron beam and the flux limitations suggest that the neutron probe is unsuited to surface studies. This is not so and evanescent neutron scattering has proven to be a valuable technique in the study of surface magnetism (Dosch, 1993).

3.3 Magnetic disorder

The high photon flux available at third-generation advanced synchrotron sources, coupled with resonant enhancement of the magnetic signal, allows the relatively weak diffuse intensities to be measured.

It is now well known that, magnetically coupled multilayers consisting of *3d* ferromagnetic layers interleaved with non-magnetic spacers exhibit giant magneto-resistance (GMR) (Baibich *et al.* 1988) for appropriate thicknesses of the non-magnetic spacer layer. These are the regimes in which the oscillatory interlayer coupling has an antiferromagnetic (AF) ground state between the ferromagnetic (F) layers. The observed change in resistivity results from the spin-dependent scattering of the conduction electrons, which depends not only on the magnetic moment alignment but also on the interfacial disorder (Zahn *et al.* 1998). Recently, the role of the structural interface morphology has attracted considerable attention because of their important role in the transport properties (Parkin, 1994). For example, structural roughness on the length scale of the interlayer magnetic coupling reduces the GMR (Shi *et al.* 1994). Given the axial nature of the magnetisation and the long range exchange interaction it is clear that the magnetic disorder need not follow exactly the

structural disorder. A detailed understanding of the interplay between structural and magnetic morphology is clearly of significance.

A forceful motivation for the study of such GMR systems is their device application possibilities. The large changes in magneto-resistance attainable with GMR heads is leading to unprecedented data storage devices. The optimisation of the GMR signal results in smaller read-heads and consequently higher areal densities. GMR devices are also candidate technologies for the next generation of magnetic random access memory (MRAM). To optimise such devices a knowledge of *magnetic* disorder and its dependence on the *structural* disorder are key.

From specular reflectivity one extracts information about the sample structure in a direction perpendicular to the sample surface. Off-specular scattering gives access to the in-plane structure of the system. Analysing the off-specular scattering within the distorted wave approximation allows a statistical measure of the height-height correlation function. These methods are complementary to direct imaging methods such as electron or atomic force microscopy, giving various statistical quantities describing the interfaces with a depth-dependent sensitivity.

The mechanisms of magnetic disorder considered here are: in-plane magnetic domains, and magnetic roughness. Magnetic roughness refers to a uniformly magnetised layer having a structurally rough interface. The magnetic “surface” will then deviate from an ideal plane and is termed *magnetic roughness*. Alternately, a non-uniform distribution of magnetisation direction is termed a *domain structure*. Both these features will produce off-specular magnetic scattering as illustrated shown in figure 10.

To study the magnetic roughness and its relation to the chemical roughness, the diffuse magnetic scattering from a Co/Cu/Co sandwich was measured by MacKay

et al. (1994). A schematic of the experimental geometry is shown in figure 11. The scattered intensity as a function of the azimuthal angle Ω is a sum of of a specular and diffuse components:

$$I(\Omega) = I_{specular}(\Omega) + I_{diffuse}(\Omega).$$

For structurally (and magnetically) flat interfaces, $I_{diffuse}(\Omega)=0$ and only specular intensity is observed. Any roughness will result in intensity scattered away from the specular direction. By tuning the incident photon energy to the Co L_3 resonance (~780eV) the scattering is now sensitive to the sample magnetisation:

$$I_{\pm}(\Omega) = I_{Structure}(\Omega) + I_{\mathrm{Re}sonant}(\Omega, M^{\pm})$$

where $M^{\pm}$ is the sample magnetisation parallel (+) or anti-parallel (-) to the incident photon helicity. To measure the asymmetry one could either change the incident photon helicity or the sample magnetisation. Experimentally, it is more convenient to reverse the sample magnetisation. The difference signal $\Delta I(\Omega, M) = I_{+} - I_{-}$ then represents the resonant contribution to the observed scattering. For identical structural and magnetic roughness ΔI will have the same form as the average signal $I_{average} = (I_{+} - I_{-})/2$. If the magnetic interface is not equivalent to the structural one the diffuse contributions may have different lineshapes, corresponding to a different power spectrum and length scale. Figure 12 shows the normalised specular and diffuse scattering for a Co/Cu/Co trilayer. For the specular reflection both $I_{average}$ and ΔI have the same form. This is expected since $\Delta I_{Specular}$ arises from the bulk magnetic scattering. In the diffuse tails the magnetic contribution is both weaker and sharper than the structural equivalent. Analysis of the scattering with in a simple kinematic picture gives a structural rms roughness and correlation length of $\sigma_{Structural} = 0.3\,\mathrm{nm}$ and $\varepsilon_{Structural} = 13 \pm 1\,\mathrm{nm}$, respectively. Analysis of the magnetic scattering gives

$\sigma_{Magnetic} = 0.15\,\text{nm}$ and $\varepsilon_{Magnetic} = 19 \pm 6\,\text{nm}$. In the trilayer and single layer samples investigated the magnetic interface is both less rough and is correlated over a greater length scale than the structural interface. The reason for this effect is not fully understood. Possible explanations range from pinning of the interfacial moments by the adjacent layer to enhanced interfacial orbital moments. McKay *et al.* suggest a coupling of the interfacial moments to the bulk moments which depends on the structural roughness. The short wavelength correlations are unable to follow the bulk magnetisation and so do not contribute to the resonant signal. To further elucidate this question, measurements on systems with controlled surface roughness show a strong correlation between the magnetic and structural interfacial roughness (Freeland *et al.* 1998). Interestingly, this technique allows one to measure separately the magnetic hysteresis loop for the bulk and interfacial contribution.

So far we have only considered magnetic roughness. On a larger length scale one must consider domain structures, typically several microns in size. Again, scattering techniques are able to quantify the degree of vertical correlation (Idzerda *et al.* 1999) of such systems. Potentially the most significant technological developments can be made in the area of magnetic spectroscopy coupled with microscopy. Typically, more conventional microscopies have been employed, such as secondary electron microscopy with polarisation analysis (SEMPA) and magnetic force microscopy. The capabilities of the x-ray technique - element specificity, a sensitivity to orbital and spin magnetisation densities and the possibility of applying large magnetic-fields make this a most important tool, especially if the lateral spatial resolution can be reduced to <10nm. A review of the present (and future) possibilities for soft x-ray magnetic research at third-generation light sources has been presented by Kortright *et al.* (1999).

Conclusions

In this chapter we have briefly reviewed the experimental exploitation and the relevant theoretical framework of the resonant magnetic scattering of x-rays (XRMS). Given the youthfulness of the technique, XRMS has made a remarkable impact on an extremely broad spectrum of magnetism research. This ranges from hard x-ray studies of magnetic structures and phase transitions to soft x-ray studies of transition metal recording media. Historically, many of these measurements have been driven by previous neutron scattering measurements. The complementarity of the two scattering techniques has provided enormous insight and will, we believe, be a very significant feature of future research directions. More recently, the element and energy band specific nature of the XRMS probe, coupled with the high brightness of third generation synchrotron sources, has led to new areas of magnetism research, inaccessible to the neutron probe,. Exciting prospects include resonant in-elastic magnetic x-ray scattering and magnetic speckle, in which an analysis of the time correlation of a speckle pattern gives access to domain dynamics with near atomic resolution, Yakhou *et al.* (1999). Clearly, the development of XRMS, coupled with magnetic spectroscopy and magnetic imaging utilising both linear and circularly polarised photons, will lead to completely new areas of magnetism research.

Figures:

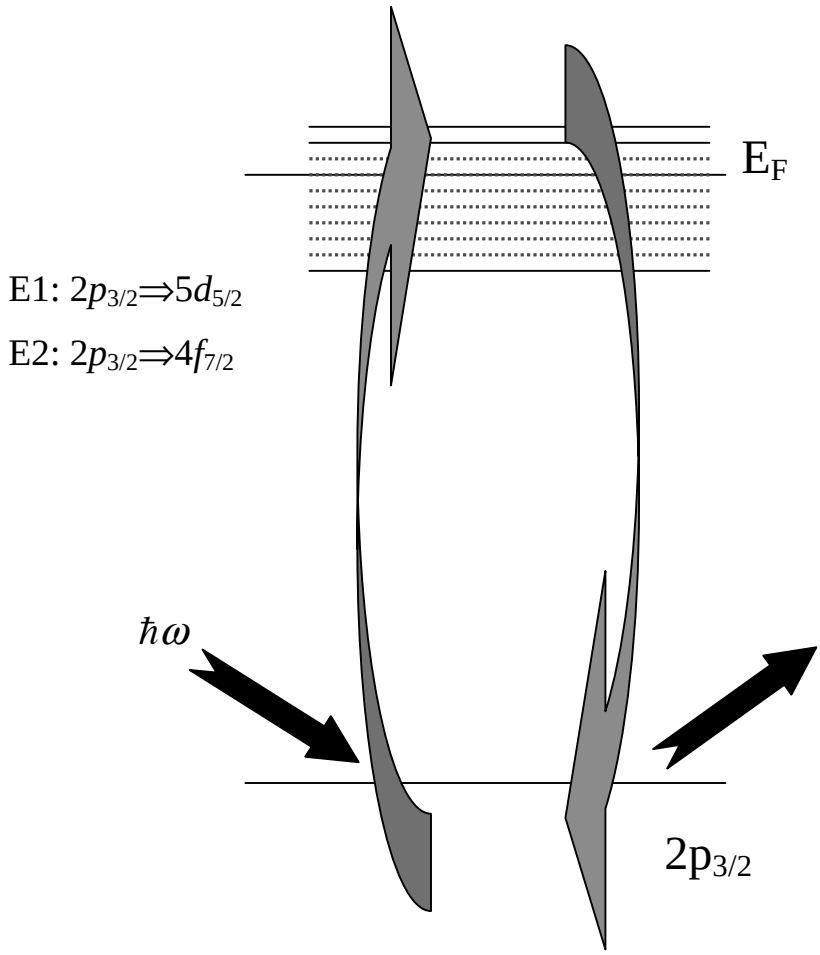

Figure 1: A schematic representation of the single electron resonant process for a rare-earth L_{III} transition. The $2p_{3/2}$ electron is excited into an unfilled level above the Fermi level (E_F) by the incident photon with energy $\hbar\omega$. The virtually excited electron decays into the core hole and emits a photon. Modified with permission from Gibbs *et al.* (1999).

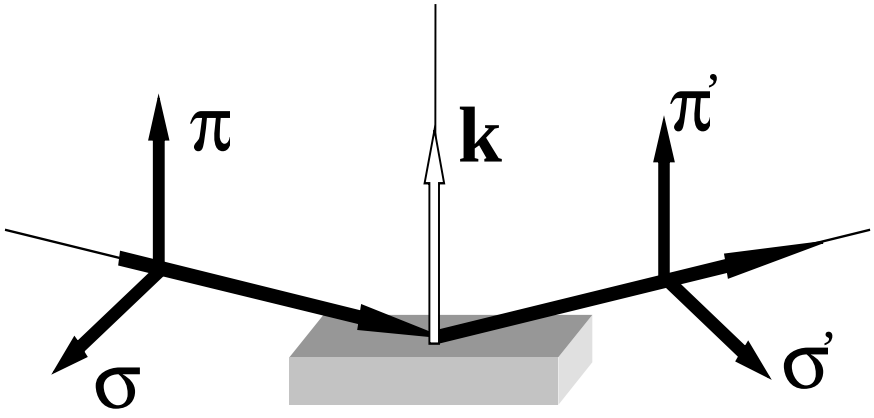

Figure 2 The scattering geometry for diffraction used in the text. σ(π) represent the incident linear polarisation perpendicular (parallel) to the scattering plane. **k** is the scattering wavevector. The z-axis is perpendicular to the scattering plane which is spanned by (π,**k**, π') and the choice of geometry follows Brunel and de Bergevin (1981). The outgoing linear polarisation can be analysed by the choice of a suitable Bragg reflecting crystal for which the scattering angle is $2\theta=90^{o}$ at the resonance energy of interest. The cos 2θ dependence of the Thomson charge scattering then selects a single state of linear polarisation.

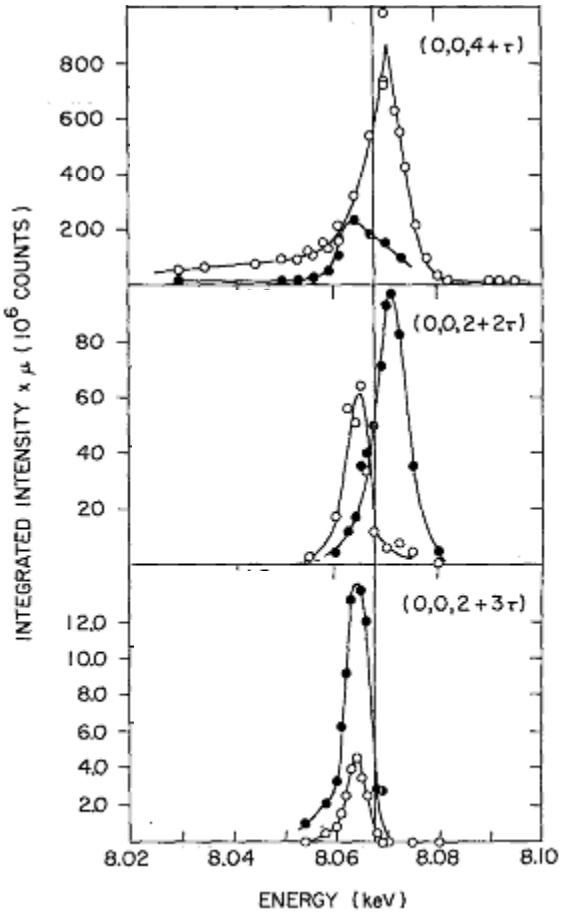

Figure 3: The integrated magnetic intensity for the scattering in the σ' (closed circles) and π' (open circles) at a series of harmonics as the energy is tuned through the Ho L_{III} edge. μ the sample X-ray absorption is not shown. Modified with permission from Gibbs *et al.* (1991).

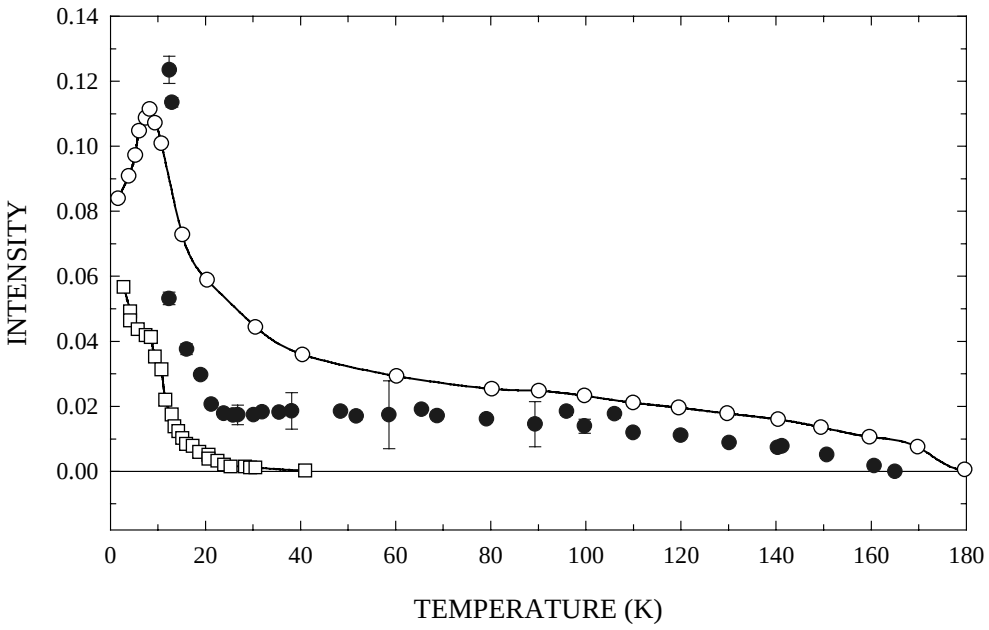

Figure 4: The temperature dependent integrated x-ray intensity for the (440)+τ measured at the Dy L_{III} (closed circles) resonance. Neutron integrated intensity for the (110)+τ (open circles) and the (121)+τ (open squares). The Dy is sited at the origin and contributes to all reflections whilst the neutron selection rule for reflections, *h* and *k* odd, is sensitive to both Dy and Fe. The reduction in the (110)+τ data at low temperature corresponds to the formation of higher harmonics of the propagation vector. Both the Dy and Fe sublattices have the same magnetic propagation vector. The solid lines are guides to the eye. Modified with permission from (Langridge et al. 1999).

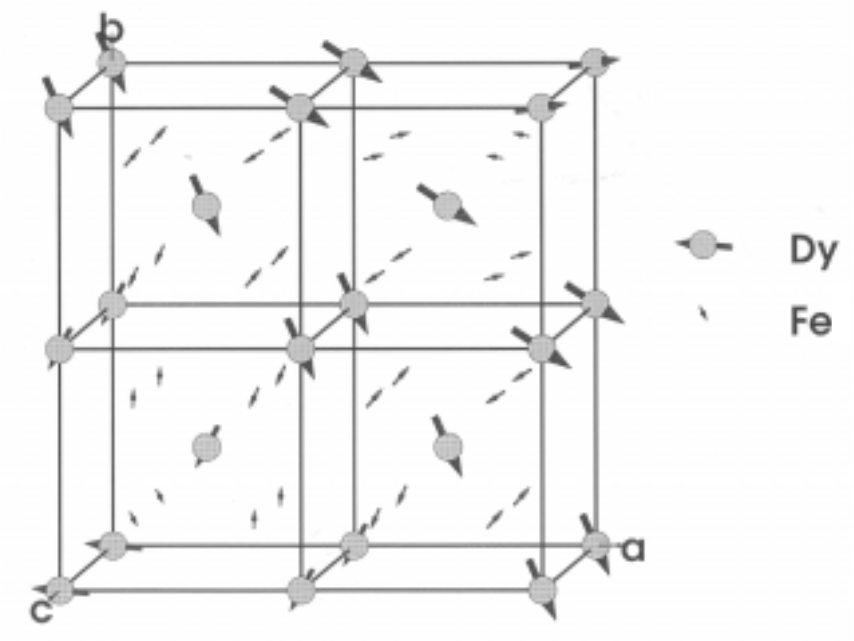

Figure 5: A model of a single domain magnetic structure of $DyFe_4Al_8$ at 17K. The propagation direction is (110). Reproduced with permission from Paixão *et al.* 2000.

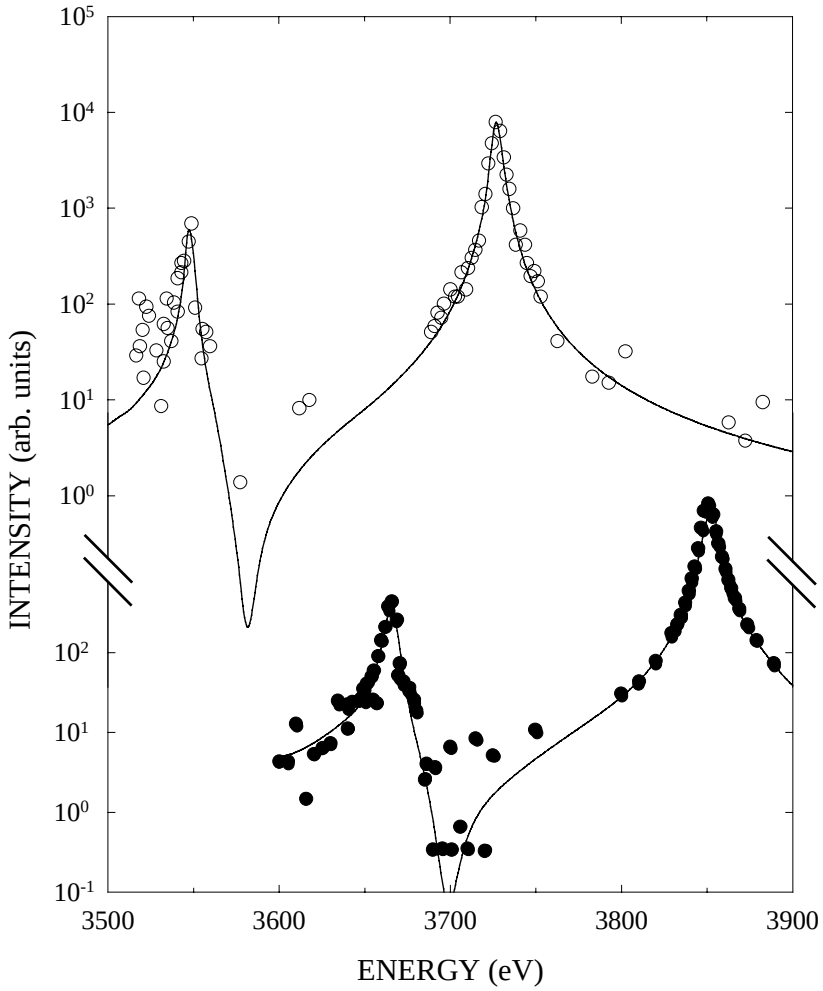

Figure 6: The absorption corrected integrated intensity for the M_4 and M_5 resonant edges of NpAs (solid circles) and USb (open circles). The solid lines are discussed in the text. Used with permission from (Langridge et al. 1994).

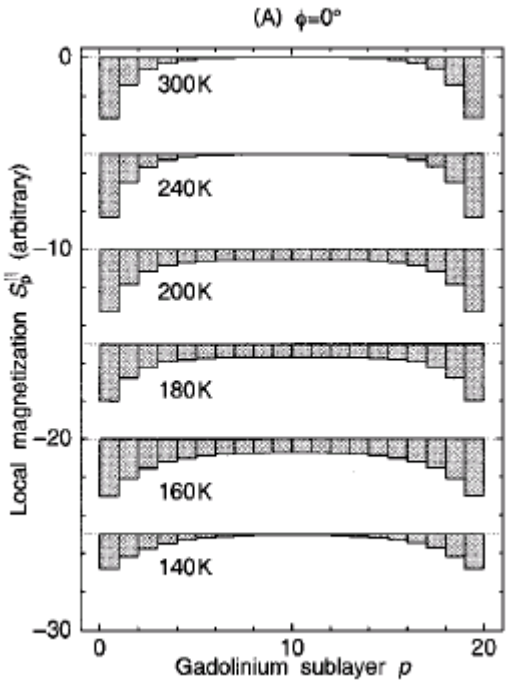

Figure 7. The modelled magnetisation for a Fe(3.5nm)/Gd(5.4nm) system as a function of temperature. A large antiparallel (to the applied field) Gd magnetisation at the interface is required to describe the observed data. Reproduced with permission from Ishimatsu *et al.* (1999).

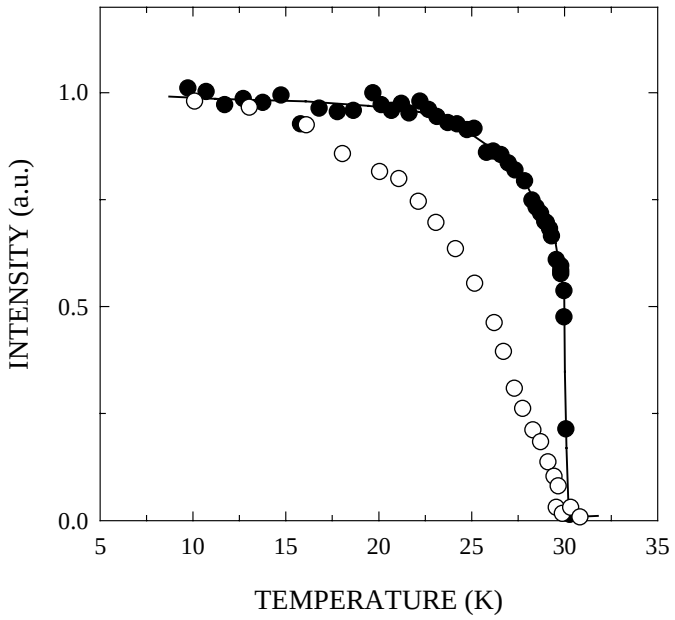

Figure 8: The normalised XRMS intensity for the (001) bulk specular Bragg reflection. The magnetic *surface* truncation rod (0 1 0.07) (open circles) exhibits a continuous phase transition. The solid line is a guide to the eye. Modified from Watson *et al*. 1996 with permission.

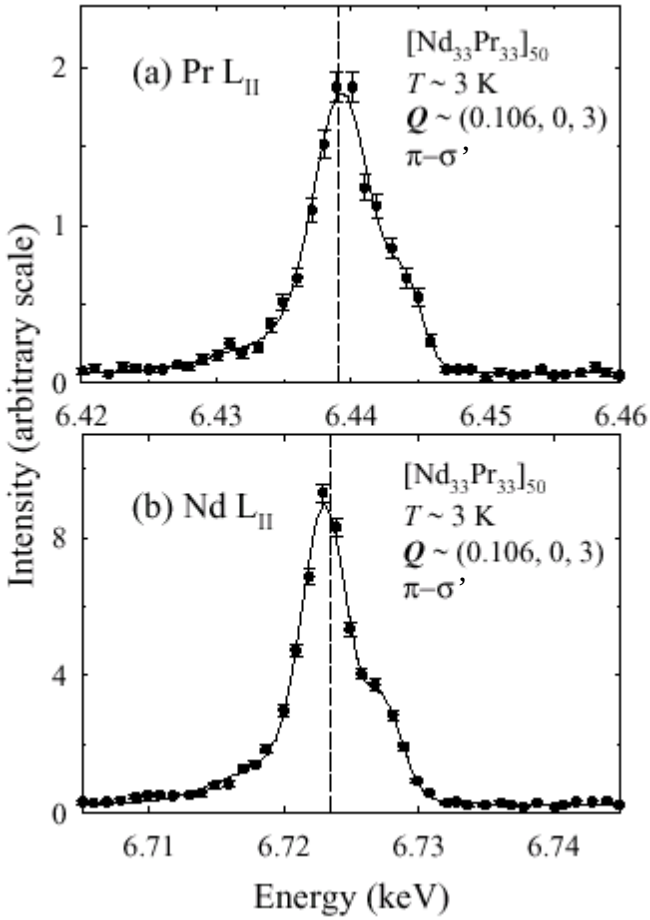

Figure 9: The XRMS at the Pr (a) and Nd (b) L_{II} edges. The solid lines are a guide to the eye. The dashed line indicates the positions of the absorption edges. With permission from Goff *et al.* (1999).

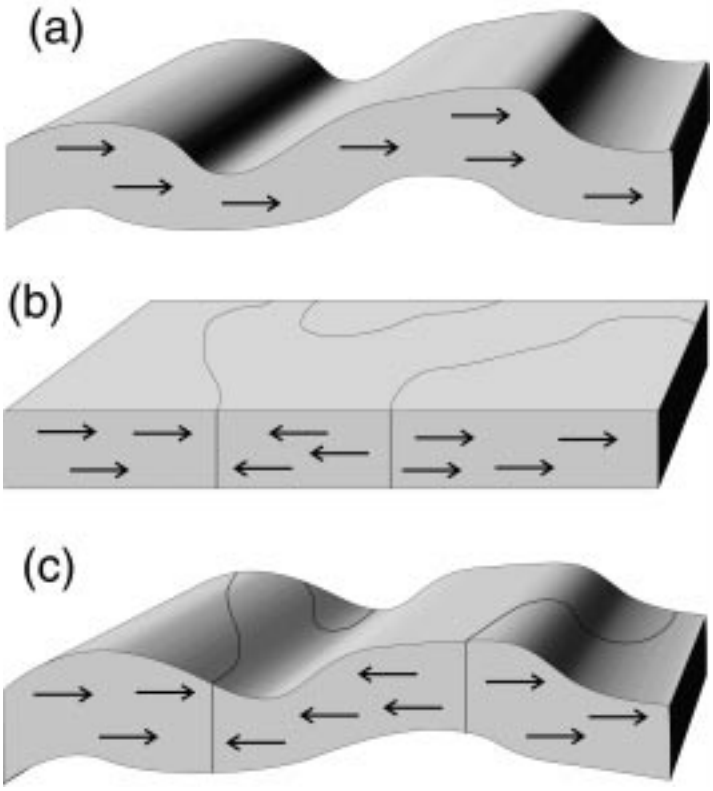

Figure 10: A schematic representation of the mechanisms giving rise to diffuse scattering. (a) A uniformly magnetised layer which is structurally rough. (b) A magnetic domain structure. (c) In physical systems a combination of both mechanisms may be present.

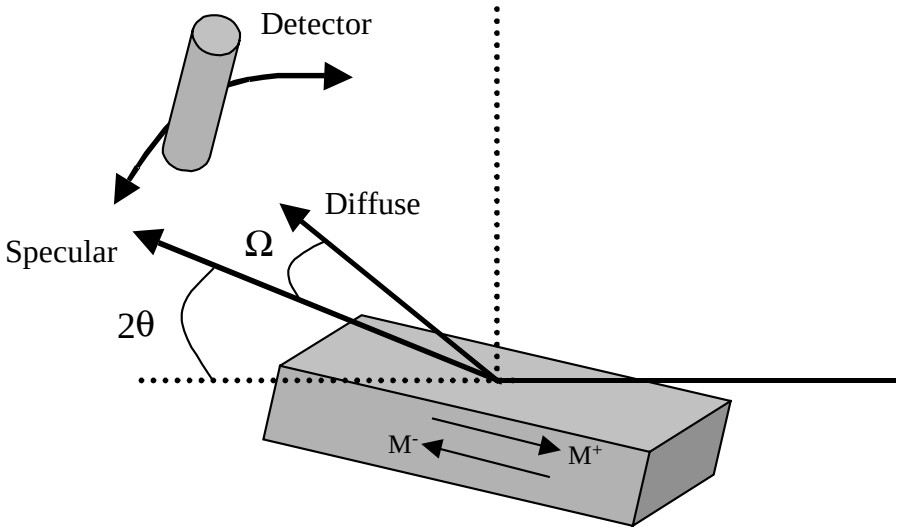

Figure 11: The scattering geometry for the diffuse measurements described. 2θ is the scattering angle and Ω is the azimuthal angle out of the scattering plane. The sample magnetisation can be controlled to be parallel (M^+) and anti-parallel (M^-) to the incident photon helicity. Modified with permission from MacKay *et al.* (1994).

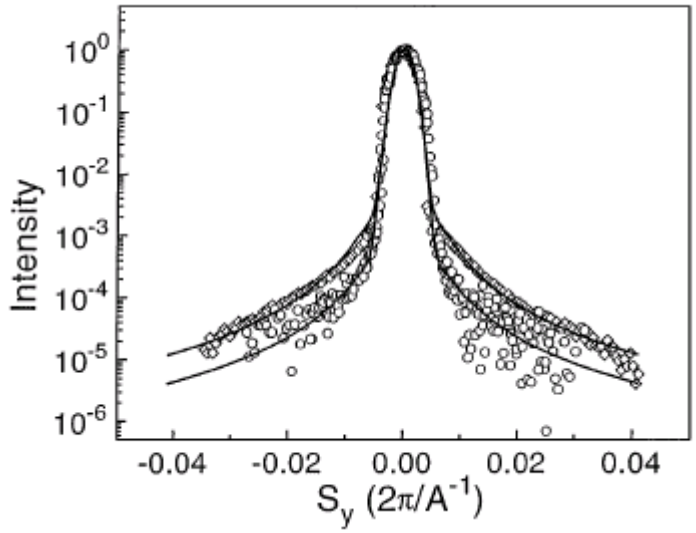

Figure 12: The normalised scattered intensity as a function of the in-plane momentum transfer from a Co(2nm)/Cu(1nm)/Co(2nm) trilayer. The magnetic contribution, ΔI (diamonds), is clearly less rough and is correlated over a longer length scale than the structural equivalent, $I_{Average}$ (circles). Reproduced with permission from MacKay *et al.* (1994).

References:

Baibich M.N. *et al.* (1988) Phys. Rev. Lett. vol 61 pp 2472

Bernhoeft N. *et al.* (1998) Phys. Rev. Lett. vol 81 pp 3419

Bernhoeft N. (1999) Acta Cryst. A. vol 52 pp 274

Bhatt G et al. (1983) Phys. Rev. **A28**, 2195

Birss RR (1964) Symmetry and Magnetism, Amsterdam: North-Holland Publ. Co.

Brunel M and DeBergevin F (1981) Acta Cryst. **A37**, 324

Carra P and Thole BT (1994) Rev. Mod. Phys. **66**, 1509

DeBergevin F and Brunel M (1981) Acta Cryst. **A37**, 314

Detlefs C. *et al.* (1996) Phys. Rev. B. vol 53 pp 6355-6361

Durbin SM (1998) Phys. Rev. **B57**, 7595

Ebert H. (1996) Rep. Prog. Phys. **59**, 1665

Finkelstein KD et al. (1992) Phys. Rev. Lett. **69**, 1612

Ferrer S. *et al.* (1996) Phys. Rev. Lett. vol 77, pp 747

Forgan E.M. *et al.* (1996) Phys. Rev. B. vol 53 pp 726-730

Freeland J.W. *et al* (1998). J. Appl. Phys. Vol 83 pp 6290

García J. *et al*. (2000) Phys. Rev. Lett. **85**, 578

Gell-Mann M and Goldberger ML (1954) Phys. Rev. **96**, 1433

Gibbs, D. *et al*. (1985) Phys. Rev. Lett., vol. 55, pp. 234-237

Gibbs, D. *et al.* (1988) Phys. Rev. Lett. vol 61, pp 1241

Gibbs, D. *et al.* (1991) Phys. Rev. B. vol 43, pp 5663-5681

Gibbs D. *et al.* (1999) *Third Generation Hard X-ray synchrotron Sources* John Wiley & Sons, New York

Goff J.P. *et al.* (1999) J. Phys C. vol 11 pp L139-L146

Goff J.P. *et al.* (2000) Physica B vol 283 pp 180-183

Grotch J et al. (1983) Phys. Rev. **A27**, 248

Hannon, J. P. *et al.* (1988) Phys. Rev. Lett. vol 61 pp 1245-1248

Hill J.P. *et al.* (1995) Phys. Rev. B. vol 52 pp 6575

Hill J.P. *et al.* (1997) Phys. Rev. B vol 55 pp R8662-8665

Hill J.P. *et al.* (1998) Phys. Rev. Lett. **80**, 4967

Hill J.P. *et al.*(2000) Phys. Rev. B. vol 61 pp 1251-1255

Idzerda Y.U. *et al.* (1999) Phys. Rev. Lett. vol 82 pp 1562

Isaacs E.D. *et al.* (1989) Phys. Rev. B. vol 40 pp 9336 and McWhan D.B. *et al.* (1990) Phys. Rev. B. vol 42 pp 6007-6017

Ishimatsu N. *et al.* (1999) Phys. Rev. B. vol 60 pp 9596-9606

Jensen, J. & Mackintosh, A.R. (1991) *"Rare-Earth Magnetism"*, Oxford Science Publications

Kokubun *et al*. (1998) J. Phys. Soc. Jpn. **67**, 3114

Kortright J.B. *et al.* (1999) J. Mag. Mag. Mat. Vol 207, pp 7-44

Lovesey SW (1987) "Theory of Neutron Scattering from Condensed Matter", vol. 2, Oxford: Clarendon Press

Lovesey SW and Balcar E (1996) J. Phys.: Condens. Matter **8**, 10983

Lovesey SW and Collins SP (1996) "X-ray scattering and absorption by magnetic materials", Oxford: Clarendon Press

Lovesey SW and Balcar E (1997) J. Phys.: Condens. Matter **9**, 4237

Lovesey S.W. (1998) J. Phys. C. vol 10 pp 2505

Lovesey SW and Knight KS (2000) J. Phys.: Condens. Matter **12**, L367

Langridge, S. *et al.* (1994) Europhysics Letters vol 25 pp 137

Langridge S. *et al.* (1999) Phys. Rev. Lett. vol 82 pp 2187-2190

Lidström E. *et al.* (2000) Phys. Rev. B. vol 61 pp 1375-1385

MacKay J.F. *et al.*(1996) Phys. Rev. Lett. vol 77 pp 3925

Mannix. D. *et al.* (1999) Phys. Rev. B. vol 60 pp 15187-15193

Murakami Y. *et al.* (1998) Phys. Rev. Lett. vol 80 pp 1932-1935

Nagano T. *et al*. (1996) J. Phys. Soc. Jpn. vol 65, 3060

Namikawa K. *et al.*(1985) J. Phys. Soc. Jpn. vol 54 pp 4099

Neubeck *et al.* (1999) Phys. Rev. B vol 60 pp R9912-9915

Nye JF (1960) Physical Properties of Crystals, Oxford: Clarendon Press

Paixão J.A. *et al.* (1993) Phys. Rev. B. vol 47 pp 8634

Paixão J.A. *et al.* (2000) Phys. Rev. B.vol 61 pp 6176-6187

Paolasini L. *et al*. (1999) Phys. Rev. Lett. 82, 4719 and Annual Report Hightlights, ESRF, Grenoble, France (1999).

Parkin S.S. (1994) *"Ultrathin Magnetic Structures II"*, Springer-Verlag, Berlin

Platzman PM and Tzoar N (1970) Phys. Rev. **B2**, 3556

Rossat Mignod J.M. (1987) "Methods of experimental physics", vol 23C, Academic Press, New York

Sakai N and Ôno K (1976) Phys. Rev. Lett. **37**, 351

Sakai N (1996) J. Appl. Cryst. **29**, 81

Shi Z.P. *et al.* (1994) Phys. Rev. B. vol 49 pp15159

Stirling W.G. and McEwen K.A. (1987) "Methods of experimental physics", vol 23C, Academic Press, New York

Stirling W.G. & Cooper M.J. (1999) J. Mag. Mag. Matl. vol 200 pp 755-773

Stunault A. *et al.* Phys. Rev. B. vol 60 pp 10170-10179

Templeton DH and Templeton LK (1994) Phys. Rev. **B49**, 14850

Van der Laan G (1994) J. Phys. Soc. Jpn. **63**, 2393

Watson D. *et al.* (1998) Phys. Rev. B. vol 57 pp 8095

Yakhou F. *et al.* (1999) ESRF Newsletter, Available: http://www.esrf.fr/info/science/newsletter/apr99/pdf/pages12to13.pdf (Accessed: August 2000)

Zahn P. *et al.* (1998) Phys. Rev. Lett. vol 80 pp 4309

Zimmermann M. v. (1999) Phys. Rev. Lett. vol 83 pp 4872-4875